



**HAL**  
open science

## Modification of $\beta$ -gallium oxide electronic properties by irradiation with high-energy electrons

T.-Huong Dang, M. Konczykowski, H. Jaffrès, V I Safarov, H.-J. Drouhin

► **To cite this version:**

T.-Huong Dang, M. Konczykowski, H. Jaffrès, V I Safarov, H.-J. Drouhin. Modification of  $\beta$ -gallium oxide electronic properties by irradiation with high-energy electrons. *Journal of Vacuum Science & Technology A*, 2022, 40 (3), pp.033416. 10.1116/6.0001821 . hal-03799721

**HAL Id: hal-03799721**

**<https://hal.science/hal-03799721>**

Submitted on 17 Oct 2022

**HAL** is a multi-disciplinary open access archive for the deposit and dissemination of scientific research documents, whether they are published or not. The documents may come from teaching and research institutions in France or abroad, or from public or private research centers.

L'archive ouverte pluridisciplinaire **HAL**, est destinée au dépôt et à la diffusion de documents scientifiques de niveau recherche, publiés ou non, émanant des établissements d'enseignement et de recherche français ou étrangers, des laboratoires publics ou privés.

# Modification of $\beta$ -gallium oxide electronic properties by irradiation with high-energy electrons

T.-Huong Dang,<sup>1</sup> M. Konczykowski,<sup>1</sup> H. Jaffrès,<sup>2</sup> V. I. Safarov,<sup>1</sup> and  
H.-J. Drouhin<sup>1,a)</sup>

<sup>1</sup>Laboratoire des Solides Irradiés, Ecole Polytechnique, CEA/DRF/IRAMIS, CNRS, Institut Polytechnique de Paris, 91128 Palaiseau, France

<sup>2</sup>Unité Mixte de Physique, CNRS, Thales, Université Paris-Saclay, 91767 Palaiseau, France

<sup>a)</sup> Electronic mail: [henri-jean.drouhin@polytechnique.edu](mailto:henri-jean.drouhin@polytechnique.edu)

We present a study of the modifications of the electronic properties of  $\beta$ -gallium oxide crystals by 2.5-MeV electron irradiation. This type of irradiation produces exclusively local point defects in  $\text{Ga}_2\text{O}_3$ , predominantly gallium vacancies which act as acceptor centers. Starting with a highly  $n$ -doped sample, we establish a quantitative linear relation between the irradiation dose and the concentration of generated acceptor centers. This gives the possibility to tune the Fermi level position within the band gap by choosing an appropriate irradiation dose. At high doses, with a very deep position of the Fermi level, the  $n$ -type sample becomes compensated, reaching a semi-insulating state. The downward shift of the Fermi level with irradiation allows us to reveal the presence of latent impurities of transition metals (like Cr and Fe) which are inactive in electron paramagnetic resonance and luminescence spectra of pristine samples. This study confirms the potential of electron irradiation as a tool for tailoring the electronic properties of gallium oxide.

## I. INTRODUCTION

Gallium oxide is an emerging ultra-wide band gap (UWBG) semiconductor, with  $E_g \sim 4.8$  eV, which has the potential to revolutionize high-power electronics due to its unusually large Baliga figure of merit<sup>1,2</sup>. Ground-breaking applications to solar-blind UV detection can be expected as well. Major international efforts are presently underway to master the material properties, a challenge remaining obtaining a *p*-type material that would open the way to bipolar structures. However, gallium oxide still remains an exploratory material on which several review papers and books have been published in recent years<sup>3-6</sup>.

In the present article, we introduce high-energy electron (HEE) irradiation as a valuable tool to investigate this new-material physics. Unlike irradiation with heavy particles, e.g. protons, neutrons or ions, which generate complex defects and extended disorder<sup>7</sup>, this type of irradiation produces exclusively point-like defects. The impinging high-energy electrons, in the MeV range, transfer to the lattice atom quite small amount of energy, just sufficient to eject an atom from its lattice site, creating Frenkel vacancy–interstitial pairs<sup>8-10</sup>. Having quite low energy barrier for migration, the interstitials migrate and annihilate on warming up the sample to room temperature, leaving behind much more stable vacancies<sup>11</sup> (annealing at rather high temperature, well above ambient temperature, is needed to remove this vacancy-type disorder). The concentration of produced vacancies essentially depends on the irradiation dose and, in this way, can be precisely controlled. The HEE-irradiation technique is non-destructive and the samples can be reset to their initial state after appropriate thermal treatment.

Transport measurements, e.g., Hall effect, as well as contactless techniques like photoluminescence (PL) and electron paramagnetic resonance (EPR) are used in the present study to monitor the evolution of material parameters versus irradiation dose. The lattice defects in semiconductors act as dopants (donors or acceptors). We demonstrate that irradiation by 2.5-MeV electrons of *n*-type  $\beta$ -Ga<sub>2</sub>O<sub>3</sub> produces a reduction of the free-carrier concentration that is indicative of the preferential introduction of acceptor-type gallium vacancies. Thus, HEE irradiation makes it possible to tune the free-carrier concentration in the sample, in particular to compensate electrically-active impurities initially present in the non-irradiated sample<sup>12</sup>. Starting from a *n*-type heavily-doped semiconductor, we obtained controlled compensation and reach an insulating state.

The introduction of acceptor-like centers produces a downward shift of the Fermi level and, in this way, helps to reveal latent impurities. Gradual modification of electronic properties, ending with an insulating state, induces important changes in EPR and optical spectra due to the modification of the charge state of latent impurities in irradiated samples.

A striking feature is that the physics observed in this UWBG semiconductor at room temperature has strong analogies with usual physics of smaller gap semiconductors, e.g., silicon, at very low temperatures.

## **II. EXPERIMENTAL**

### ***A. Samples and Irradiation***

In our experiments, we used commercially available  $\beta$ -Ga<sub>2</sub>O<sub>3</sub> crystalline substrates from Novel Crystal Technology Inc<sup>13</sup>. We deal with two types of 650- $\mu$ m-thick substrates

(i) *n*-type Sn-doped with electron concentration in the range  $2\text{-}3 \times 10^{18} \text{ cm}^{-3}$  and (ii) unintentionally doped (UID) with  $(N_D - N_A) \sim 3 \times 10^{17} \text{ cm}^{-3}$ .

Irradiation with 2.5-MeV electrons was performed at the SIRIUS Pelletron NEC electrostatic accelerator operated by the Laboratoire des Solides Irradiés (LSI) at the Ecole Polytechnique, Palaiseau, France<sup>14</sup>. In order to avoid excessive heating and migration of the defects created during irradiation, the sample was cooled down to  $\sim 20 \text{ K}$  by immersion in liquid hydrogen. Uniformity of irradiation was obtained by vertical and horizontal scanning of the beam. The penetration depth of 2.5-MeV electrons into  $\text{Ga}_2\text{O}_3$  is of the order of 1cm. It largely exceeds the 650- $\mu\text{m}$  thickness of our samples thus granting a uniform distribution of the induced defects. The irradiation dose was monitored after integrating the current collected on a Faraday cup placed behind the sample.

Warming up of irradiated samples to room temperature before transfer to other experimental platforms results in partial annealing of damage: collapse of close Frenkel pairs and annihilation of interstitials via migration to the surface and to other sinks. The migration energy of the vacancies is much higher than that of interstitials; in consequence, the damage remaining at room temperature is exclusively of vacancy type. It is quite stable: we do not observe any evolution of the properties of irradiated samples stored at room temperature over several months.

The concentration of created vacancies  $N_V$  can be evaluated through the following relation:

$$N_{Vi} = \sigma_i N_i \Phi \quad (1)$$

where  $\sigma_i$  is the cross section for HEE interaction with the lattice ions,  $N_{li}$  is the concentration of the corresponding lattice ions, and  $\Phi$  is the irradiation fluence, i.e., the number of high-energy electrons impinging on a unit area of the sample. The index  $i$  refers to the chemical sublattice (gallium or oxygen) relevant to the selected parameter. In our experiments, we characterize the HEE fluence through the irradiation dose: the amount of electronic charge (measured in milli-Coulombs) received per unit area on the sample surface (measured in  $\text{cm}^2$ ).

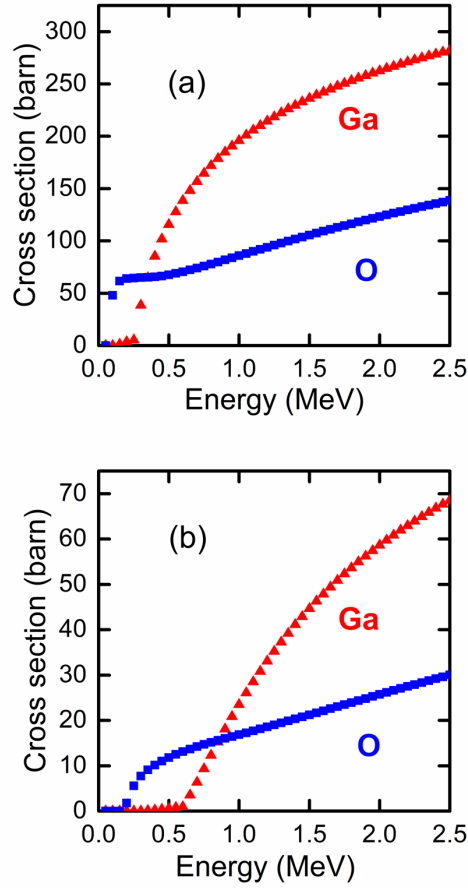


FIG. 1. Calculated cross sections  $\sigma$  for Frenkel-pair production in the gallium (red triangles) and oxygen (blue squares) sublattices of Ga<sub>2</sub>O<sub>3</sub> as a function of the electron energy  $E_e$ : simulation with the SECTE program (Ref. 16) with a displacement-energy parameter taken as: (a) 10 eV; (b) 30 eV.

The cross section  $\sigma_i$  for the creation of a Frenkel pair depends on the chemical origin of the lattice ion and on the energy of the incoming electrons  $E_e$ . Energy transfer from an impinging swift electron with 2.5-MeV energy to the crystal lattice is mainly of Rutherford-collision type. The alternative channel of energy transfer by electronic excitations is negligible as evaluated by NIST ESTAR simulator<sup>15</sup>. With the SECTE software developed at LSI<sup>16</sup>, we estimated the cross-sections  $\sigma$  for formation of Frenkel pairs in gallium and oxygen sublattices as a function of incident electrons energy  $E_e$ . The unknown parameter in these calculations is the displacement threshold  $E_{dt}$ , the minimal amount of energy transferred to an atom in a Rutherford collision that is needed to break the chemical bonds<sup>17</sup>.

Figure 1 shows the  $\sigma_i (E_e)$  relations for Ga and O sublattices, the  $E_{dt}$  energies being taken as 10 and 30 eV. The general shape of the  $\sigma_i (E_e)$  curves is similar for different energies  $E_{dt}$ , only the exact numerical values varying. The calculated values of  $\sigma_i$  (2.5 MeV) for several  $E_{dt}$  parameters are represented in Fig. 2.

The oxygen vacancies  $V_O$  in  $Ga_2O_3$  are predicted to be (deep) donor-type dopants<sup>18,19</sup>. On the contrary, the gallium vacancies  $V_{Ga}$  are expected to give acceptor-like levels in the forbidden gap<sup>19-21</sup>. On the basis of the  $\sigma_i (E_e)$  variations presented in Fig. 1, we can expect that HEE irradiation with electron energy less than 0.5-MeV would exclusively produce donor-type doping by oxygen vacancies. In our case of a 2.5-MeV beam energy, irradiation simultaneously produces gallium and oxygen vacancies. However, the rate of creation of  $V_{Ga}$  is about twice that of  $V_O$ . Thus, we would expect that 2.5-MeV irradiation overall produces an acceptor-type doping.

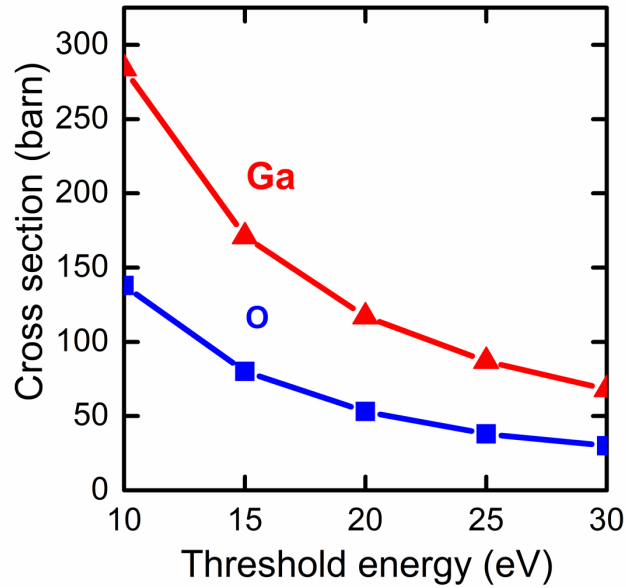


FIG. 2. Variation of cross sections  $\sigma_i$  (2.5 MeV) versus displacement energy for gallium (red triangles) and oxygen (blue squares) sublattices.

A rough estimate of the concentration of induced defects can be obtained from Eq.

1. Assuming a threshold energy  $E_{dt} = 25$  eV for displacement of Ga atoms under 2.5-MeV electron impact, and a related  $\sigma$  value of 90 barn, we estimate that irradiation at 1.0 mC/cm<sup>2</sup> dose would create gallium vacancies with a concentration of  $1.2 \times 10^{16}$  cm<sup>-3</sup>. This corresponds to a brief 70-sec irradiation under standard conditions with 3- $\mu$ A beam current, on an area limited to 0.2 cm<sup>2</sup> through a 5 mm diameter diaphragm.

### **B. Characterization methods**

We essentially used three techniques to characterize the modifications of electronic properties of the material induced by HEE irradiation: electrical measurements, which relate to the concentration of free charge carriers, their mobility and its temperature dependence; PL spectroscopy, which gives the spectrum of electron levels in the

forbidden gap, and EPR spectroscopy, which provides information on paramagnetic impurity centers in the crystal.

Electrical characterizations mostly refer to conductivity and Hall measurements by van der Pauw method using a Linear Research LR700 AC Resistance Bridge.

The PL studies at room temperature were performed with a Fluorolog-5 (HORIBA JOBIN YVON) spectrofluorimeter. In some experiments, we used an optical excitation with a 266-nm pulsed laser (INDI-40-10 HG, Spectra-Physics) or a 4-mW blue semiconductor laser diode emitting at 450 nm.

The EPR spectra were measured with a JEOL-JES310 spectrometer at ambient and 100-K temperatures.

### **III. RESULTS AND DISCUSSION**

#### **A. *Electronic transport***

Electrical transport measurements were realized on highly doped *n*-type samples ( $\sim 2 \times 10^{18} \text{ cm}^{-3}$ ) in which we were able to monitor the variation of electrical properties after sequential irradiation with increasing doses.

In the first step of sample preparation required for electrical measurements,  $2 \times 2\text{-mm}^2$  square samples were cut with a diamond coated wire saw from the 0.65-mm-thick substrates. Additional cut parallel to the surface reduced the sample thickness to about 200  $\mu\text{m}$ . Electrical point contacts were deposited by evaporation of Ti: Au layers through a shadow mask. The ohmic character of the contacts was established after annealing in air at 325°C. The contacts produced according to this procedure remained ohmic upon cooling from room temperature down to 100 K. However, below this temperature the

ohmic characteristics of contacts were strongly affected, jeopardizing reliable conductivity measurements below 100 K.

The main sample surface corresponded to the (010) crystallographic plane containing the two [100] and [001] crystallographic directions. In the van der Pauw geometry, the electrical point contacts deposited on the corners were aligned along these two directions. In all measurements, we did not find any indication of conductivity anisotropy, the van der Pauw factor always remaining very close to unity as expected for an electrically-isotropic square sample. This conclusion agrees with previously reported observations of electronic transport in  $\text{Ga}_2\text{O}_3$ <sup>22</sup>.

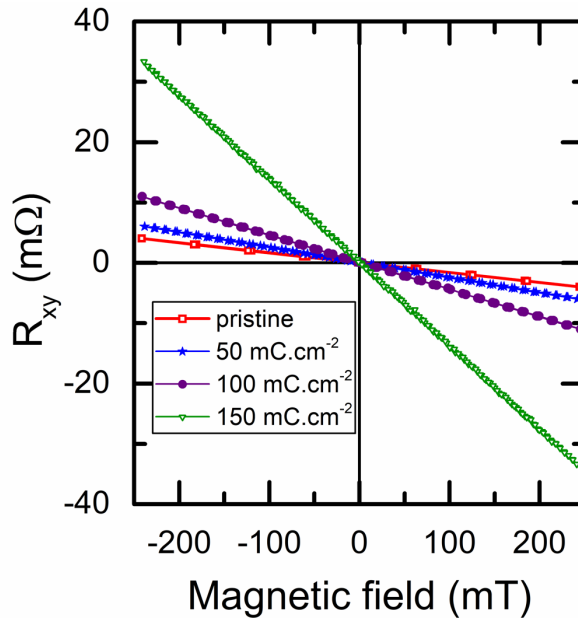


FIG. 3. Hall resistance  $R_{xy}$  versus magnetic field for a sample irradiated with increasing doses.

In the van der Pauw geometry, the Hall effect in a magnetic field  $B$  perpendicular to the sample surface is extracted from the diagonal resistances measured with a current flowing between contacts along a diagonal of the square, the voltage being measured on

contacts located along the other diagonal. The Hall resistance  $R_{xy}$  corresponds to the difference between the two diagonal resistances measured after permutation of current- and voltage-measuring contacts. By calculating this difference, the  $R_{xx}$  contributions cancel so that the result exclusively represents the  $R_{xy}$  Hall contribution.

As shown in Fig. 3, the  $R_{xy}(B)$  variation measured at room temperature is perfectly linear, with a slope corresponding to the Hall coefficient. The rise of the Hall coefficient after irradiation is clearly seen as an increase of the slope of the  $R_{xy}(B)$  line and reflects the depletion in free-carrier concentration.

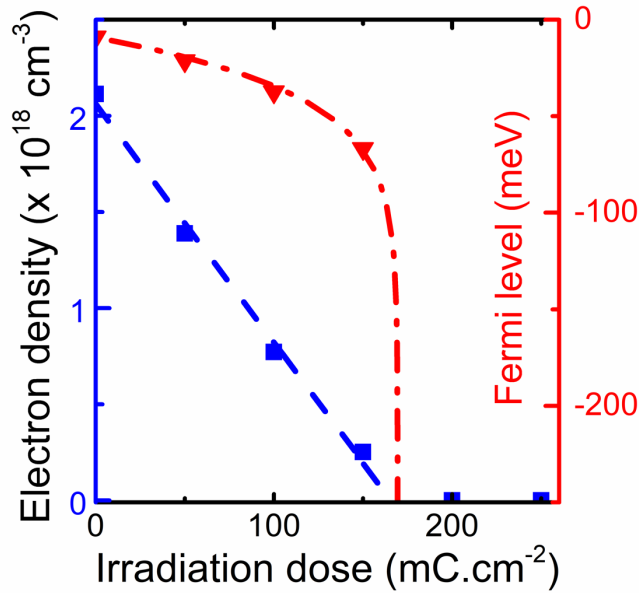


FIG. 4. Conduction-electron density of a Sn-doped  $\beta$ - $\text{Ga}_2\text{O}_3$  crystal sample (blue squares) as a function of HEE irradiation dose and calculated Fermi-level position (red triangles) below the bottom of conduction band (see Sec. III-D).

Figure 4 shows the variation of the free-carrier concentration determined from the Hall measurements in samples with increasing dose of irradiation. In the first stages of irradiation, the decrease of the carrier concentration is perfectly linear with the dose,

which allows us to quantify the effect of irradiation: a dose of  $1 \text{ mC/cm}^2$  reduces the concentration of conduction electrons by  $1.24 \times 10^{16} \text{ cm}^{-3}$ . The irradiation at high doses, exceeding  $175 \text{ mC/cm}^2$ , turns the highly-conductive initial sample with a resistivity of  $0.05 \text{ } \Omega \cdot \text{cm}$  into a nonconductive - insulating - state so that further measurements of conductivity and Hall coefficient are no longer possible on our platform.

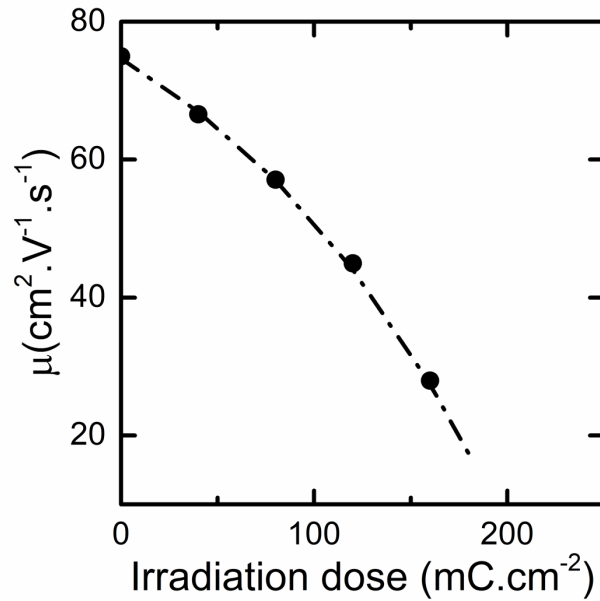


FIG. 5. Conduction-electron mobility in a Sn-doped  $\beta\text{-Ga}_2\text{O}_3$  crystal sample versus HEE-irradiation dose.

A similar linear decrease of the free-carrier concentration with irradiation dose was observed on a second sample cut from the same Sn-doped substrate. Within the error in the determination of sample thickness, the rate of depletion of the free-carrier concentration and the critical dose required to convert a sample into an insulating state were the same in both of them.

The reduction of carrier concentration in irradiated samples is accompanied by a decrease of the carrier mobility (Fig. 5) which drops from  $75 \text{ cm}^2/(\text{V}\cdot\text{s})$  in pristine

samples down to  $28 \text{ cm}^2/(\text{V}\cdot\text{s})$  after irradiation at a  $160\text{-mC}/\text{cm}^2$  dose, as measured at room temperature.

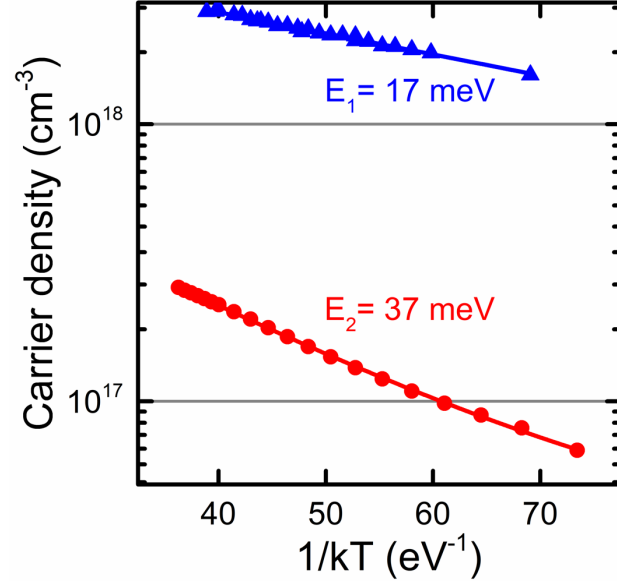


FIG. 6. Electron-density Arrhenius plots for the pristine sample (blue triangles) and for samples irradiated at  $160\text{-mC}/\text{cm}^2$  dose (red circles).

The temperature dependences of the carrier concentration reveal a thermally activated regime for electrons excited from donor states to the conduction band. Figure 6 presents Arrhenius plots for a Sn-doped sample before and after irradiation at  $160 \text{ mC}/\text{cm}^2$ . From the fitting parameters of these plots, we obtain activation energies of  $E_1 = 17 \text{ meV}$  for the pristine sample and  $E_2 = 37 \text{ meV}$  for the same sample after irradiation.

### **B. Electron paramagnetic resonance**

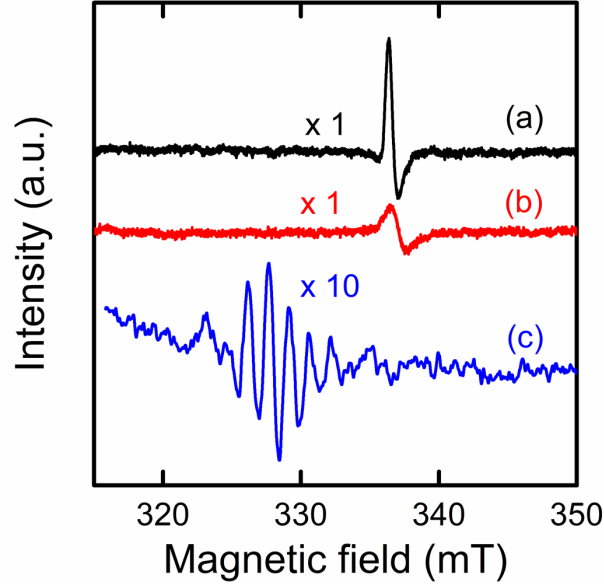


FIG. 7. EPR spectra measured at room temperature for UID  $\beta$ -Ga<sub>2</sub>O<sub>3</sub> samples: (a) pristine sample, (b) irradiated at 20-mC/cm<sup>2</sup> dose; (c) irradiated at 60-mC/cm<sup>2</sup> dose.

The observations on irradiated samples tend to confirm the conclusion made on the basis of electrical measurements. In non-irradiated UID samples, we observe a well-known very-intense and very-narrow EPR line with an electron  $g$ -factor  $g = 1.97$  as shown in Fig. 7a. This line is usually assigned to free electrons or electrons localized on shallow donors<sup>20,23-26</sup>. A weak dose of irradiation, namely 20 mC/cm<sup>2</sup>, leads to a significant reduction of the line intensity (Fig. 7b). At an irradiation dose of 40 mC/cm<sup>2</sup>, the line is no longer detectable in the EPR spectrum and, at higher irradiation doses, this EPR line is replaced by a new one showing a well-resolved hyperfine structure (Fig. 7c). This type of EPR signal was already observed in Ga<sub>2</sub>O<sub>3</sub> crystals irradiated by neutrons<sup>27</sup>, protons<sup>28</sup>, or annealed at high temperature ( $> 1400^\circ\text{C}$ ) under oxygen atmosphere<sup>29</sup>. This structure is always attributed to gallium vacancies or their complexes with other defects and strong hyperfine interaction with neighboring gallium nuclei.

It is worth to note that large-scale EPR spectra of irradiated samples (Fig. 8) also contain a number of intense lines which we attribute to transition metals ions (TMI) like  $\text{Cr}^{3+}$  and/or  $\text{Fe}^{3+}$ . Their precise interpretation needs a detailed analysis which will be presented elsewhere. According to the manufacturer's specifications, the initial UID samples indeed contain such impurities at a level of  $10^{16}$ - $10^{17}\text{cm}^{-3}$ , as checked by SIMS analysis<sup>13</sup>. However, the TMI lines are clearly seen in the spectra obtained from irradiated samples (Fig. 8b) but are hardly detectable (if even not seen at all) in pristine non-irradiated ones (Fig. 8a). This supposes that the TMIs can change their electronic configuration and capture or release extra electrons depending on the availability of free electrons in the conduction band. Only ions with the charge 3+ (like  $\text{Cr}^{3+}$  and  $\text{Fe}^{3+}$ ) are detected in EPR spectra.

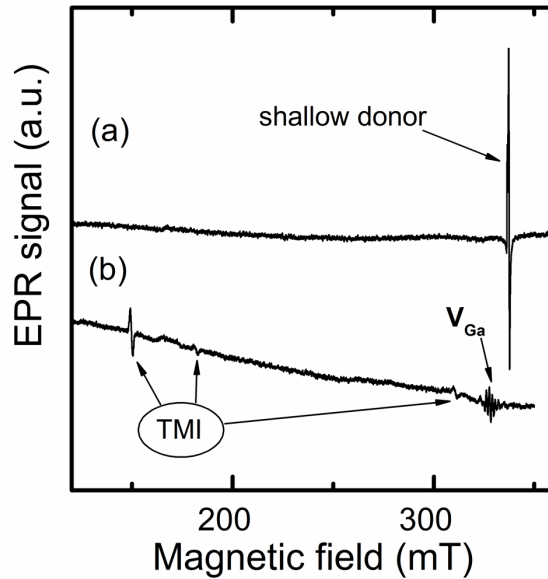


FIG. 8. Large-scale EPR spectra for UID samples at 100 K: (a) pristine sample; (b) same sample irradiated with the  $60\text{-mC/cm}^2$  dose. Peaks related to Transition Metal Ions (TMI) are evidenced.

We also observe that the irradiated samples completely recover the EPR spectra in their initial forms, characteristics of non-irradiated samples, after 30 min annealing in air at a relatively low temperature of 680°C, by far inferior to the fusion temperature of gallium oxide (~ 1800°C). This result confirms that the observed effects are due to point defects introduced by HEE irradiation and that they can be easily eliminated after appropriate thermal treatment, perfectly resetting the sample properties to their initial values.

### **C. Photoluminescence spectroscopy**

The essential features of the PL spectra of  $\beta$ -Ga<sub>2</sub>O<sub>3</sub> have been reported almost 50 years ago, in the early 1970's<sup>30-32</sup>. The spectra of a *n*-type Ga<sub>2</sub>O<sub>3</sub> crystal are rather poor and consist of quite broad overlapping bands, often labeled “UV-”, “blue” or “green” bands. The UV-band is generally attributed to the emission of self-trapped excitons and the blue band, hereafter referred to as B-band, to the recombination at donor-acceptor pairs<sup>24,33-37</sup>. These bands are excited by the 266-nm UV light (4.67 eV) very close to the steep increase in the absorption corresponding to the transition from the valence to the conduction band<sup>24,25,31,37,38</sup>. The more recent publications report the observation of the same bands and include more careful investigation of their temperature dependence<sup>24,36</sup>, decay times<sup>24</sup>, light polarization<sup>37</sup>, as well as comparison with EPR spectra<sup>24,25</sup>, electrical transport data<sup>36</sup>, and theoretical calculations<sup>34,35</sup>. However, definitive interpretations have still remained pending.

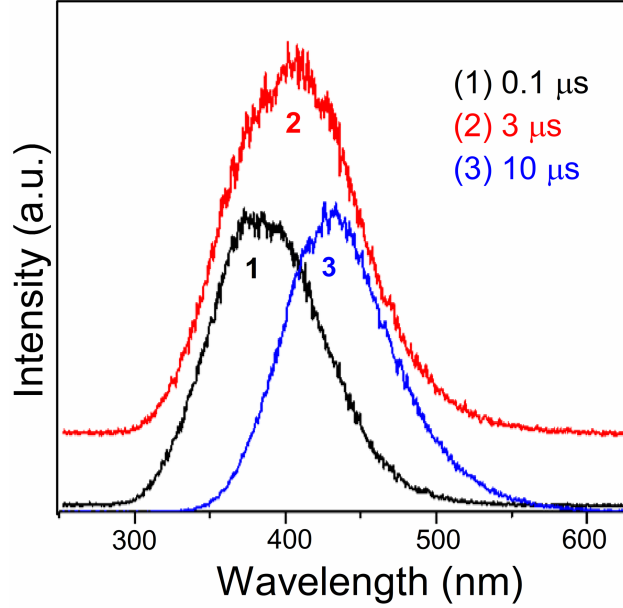


FIG. 9. Time-resolved spectra for a non-irradiated UID sample at room temperature excited by 266-nm pulsed laser: 0.1- $\mu\text{s}$  delay (black, 1); 3  $\mu\text{s}$ -delay (red, 2); 10  $\mu\text{s}$ -delay (blue, 3). The spectra taken with different delay times were normalized to their maximum values;

Our non-irradiated samples exhibit a typical 380-nm (3.3 eV) broad band which is usually observed in UID and *n*-doped samples. This band is the superposition of two strongly overlapping and rather broad bands, the UV-band at 365 nm and B-band at 480 nm (3.4 eV and 2.6 eV respectively). We were able to identify them in time-resolved spectra due to the difference of their decay times.

Figure 9 shows the spectra excited by a 266-nm pulsed laser with different delay times after excitation pulse. Besides the 270-nm peak corresponding to the near band-to-band transition, the B-band is also excited by absorption well below the band gap at around 375 nm (3.30 eV). The excitation and emission bands (Fig. 10) are symmetrically

located around presumed zero-phonon transitions at 3.03 eV with a Stokes shift equal to 0.52 eV.

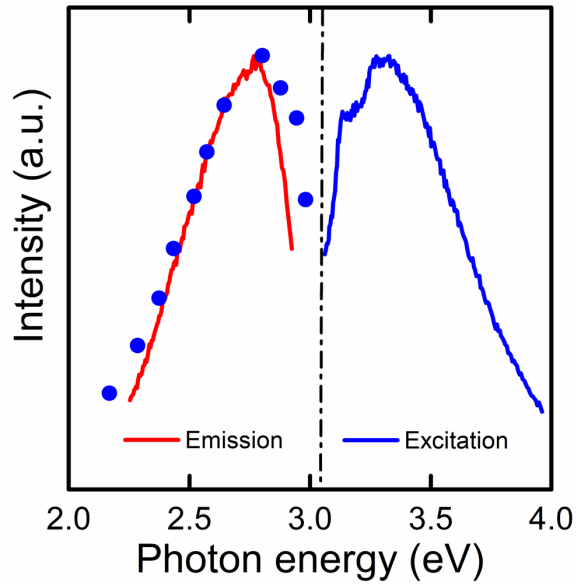


FIG. 10: Excitation-emission symmetry of the B-band spectra: the blue circles visualize the symmetric reconstruction of the excitation spectrum superimposed on the emission spectrum. The high-energy part of emission spectrum is distorted by the 420-nm edge filter introduced in order to block 375-nm excitation light.

Figure 11a presents the evolution of the emission spectra of UID samples with increasing irradiation dose at room temperature and under excitation at 270 nm in our fluorimeter. The irradiation does not change very much the spectrum components near the band gap. We observe the same UV- and B-bands. However, their intensity significantly drops with the increase of the irradiation dose. At the same time, we observe the emergence and progressive growth of new rather-narrow lines labeled  $R_1$  and  $R_2$  in the red spectral region around 690 nm. In strongly irradiated samples, these red R-lines dominate the spectrum.

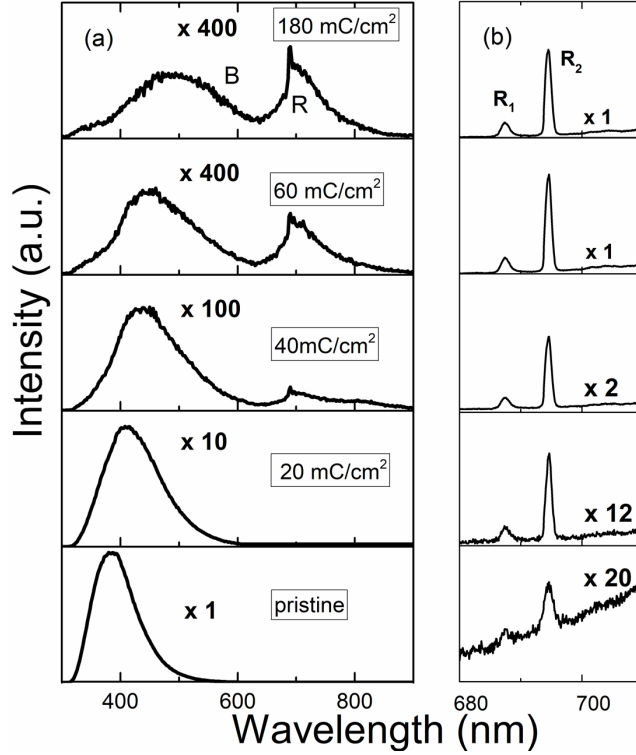


FIG. 11. (a) Room-temperature photoluminescence spectra of UID samples with different irradiation doses, detected in a fluorimeter with 270-nm excitation; (b) The R-line spectra at low temperature (100 K) of the same samples, excited with 450-nm laser diode.

Figure 12 shows the excitation spectra of the R-lines at room temperature. As can be seen, the band-to-band transition at 270 nm and absorption into self-trapped excitons, corresponding to the UV emission band contribute to the excitation of these centers. However, the most efficient process is the excitation into a very broad band peaked at 445 nm (2.8 eV) which apparently corresponds to the proper absorption of the center. The intensity of the R-lines significantly grows up when lowering the temperature and it is for this reason that we present in Fig. 11b the evolution of their intensity versus increasing irradiation dose measured at low temperature (100 K) under intra-center 450-nm excitation.

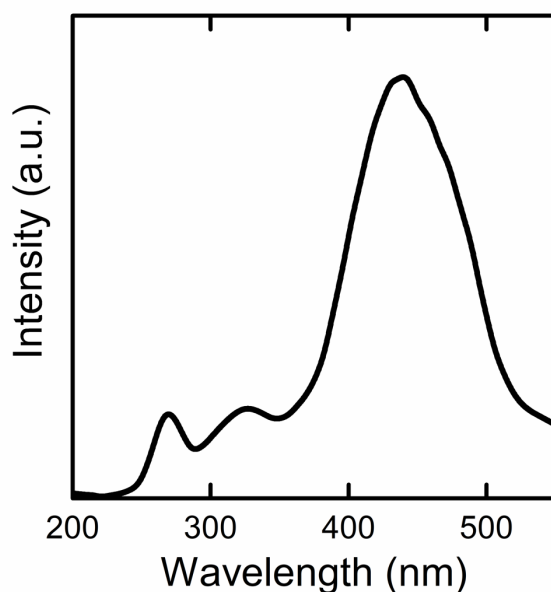


FIG. 12. Excitation spectrum of R-lines at room temperature for UID samples irradiated at  $60\text{-mC/cm}^2$  dose.

The striking feature in Fig. 11a is the very strong drop of the total luminescence intensity with increasing irradiation dose in the case of excitation through band-to-band absorption at 270 nm. In order to present spectra of the same size for all samples in Fig. 11a, we needed to enhance the spectra of strongly-irradiated samples by a factor up to  $\sim 400$ . This clearly shows that irradiation introduces or activates local defects which play the role of very efficient centers for non-radiative recombination of free carriers in the conduction and valence bands. Thus, carriers excited in the conduction and valence bands by 270-nm excitation have several channels for recombination: radiative processes related to different luminescence bands and non-radiative ones introduced by irradiation. The general form of the spectra and relative intensities of different emission bands in great part result from a competition between these different recombination channels and are dependent on the excitation intensity. The spectra in Fig. 11a correspond to a very

weak excitation in the fluorimeter (narrow spectral band of a Xe lamp, filtered by a monochromator). At higher excitation level produced by a pulsed laser, the UV-band in irradiated samples becomes more intense than other bands and dominates the spectrum. Apparently, the recombination through the B- and R-bands with quite long decay times tends to saturate at high excitation levels. In these conditions of excitation through band-to-band absorption, the intensities of different emission bands are not reliable parameters to assess the concentration of corresponding local centers.

In order to monitor the concentration variation of local centers with irradiation dose, we do prefer measuring the emission intensities of the B-band and R-lines being excited through their intra-center absorption at 375 nm and 450 nm, respectively. In this case the photo-excited electrons (holes) do not transit by the conduction (valence) band: the excitation and emission processes occur at a same local center and do not *a priori* suffer from competition with other recombination channels.

The case of the R-lines is presented in Fig. 11b. In contrast to the band-to-band excitation, where the total intensity of luminescence decreases with irradiation, the R-lines excited through their intra-center absorption increase in intensity by more than 20 times. This is also the case for the B-band, but the increase in intensity is much more modest (a factor of 2, or so).

Figure 13 summarizes the intensity variations of characteristic emission bands as a function of the irradiation dose. Note that the scale in the graph is logarithmic and the intensities of the different bands are normalized to their intensities in the non-irradiated sample. Figure 13 clearly shows the essential features of intensity variations: jump up in

intensity for intra-center excitation and drop in intensity for band-to band excitation within a rather narrow window of irradiation doses, 0-40 mC/cm<sup>2</sup>. For higher doses the variations become saturated and the emission intensities of all bands do not change any more.

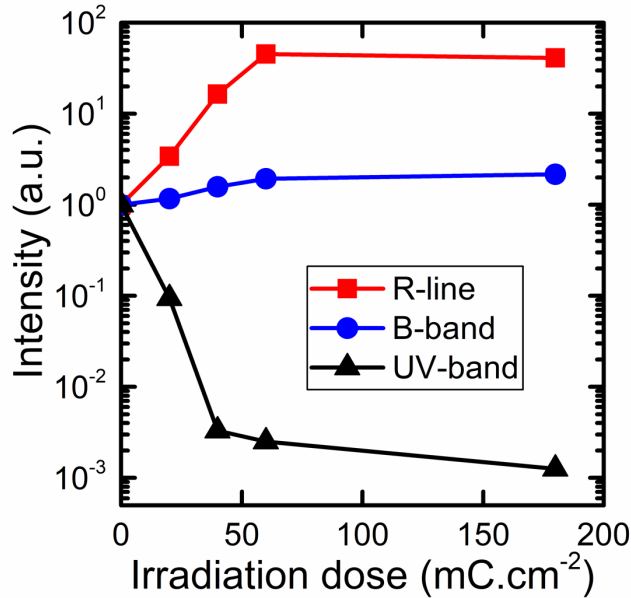


FIG.13. Intensity variation of luminescence bands as a function of the irradiation dose: the UV-band excited with a 270-nm light at room temperature (black triangles); B- band excited with a 375-nm light at room temperature (blue circles); R-lines excited by a 455-nm laser at 100 K (red squares).

As mentioned above, HEE irradiation essentially introduces lattice defects which are known to be healed by thermal annealing. In our case, regarding PL spectra and similarly EPR spectra, as reported in Sec. III-B, we observe that a 30-min annealing at 650°C in air completely eliminates all spectral changes introduced by irradiation: the UV- and B-bands recover their previous intensities and the R-lines completely disappear from the room temperature spectra.

#### **D. Discussion**

All the above-reported results clearly show that HEE irradiation strongly affects electronic properties of  $\beta$ -Ga<sub>2</sub>O<sub>3</sub> semiconductor crystals, reducing their electrical conductivity, altering PL and EPR spectra. These major changes are apparently related to the generation of a large concentration of local defects, like gallium vacancies. The situation is completely reversible since these point defects can be healed by thermal annealing at proper temperature, after which the sample recovers its pristine electronic properties.

The observed reduction in the concentration of conduction electrons in irradiated samples attests that the gallium vacancies predominately introduced by HEE irradiation produce acceptor-like levels in the forbidden band gap of the crystal. The Hall measurements presented in Sec. III-A (Fig. 4) provide quantitative evaluations of this effect: an irradiation at a 1.0-mC/cm<sup>2</sup> dose introduces  $1.24 \times 10^{16}$  cm<sup>-3</sup> of active acceptor-like centers into a gallium oxide sample. This value is very close to the rate of Ga-vacancy creation estimated from the effective cross section (Sec. II-A).

Following irradiation, the acceptor-like gallium vacancies capture electrons from Sn donors initially present in the pristine sample, thus increasing the concentration of charged defects acting as scattering centers which leads to a significant reduction of the carrier mobility observed in irradiated samples.

The modifications of the electron transport properties with irradiation can be described in terms of displacement of the Fermi level in the crystal. In initially *n*-type Sn-doped samples, the Fermi level is located near the bottom of conduction band. The introduction of acceptor-like gallium vacancies by HEE irradiation reduces the concentration of free electrons in the conduction band and provokes a downward shift of

the Fermi level. In Fig. 4a, we indicate the Fermi level position below the bottom of conduction band, calculated from data on the concentration of conduction electrons in the framework of the effective mass approximation, the effective mass of electrons being taken as  $m_e = 0.28 m_0$  (Ref. 19). A smooth downward shift of the Fermi level at small doses is followed by a sharp drop of its position when approaching complete compensation of the existing donors by acceptor-like centers introduced by irradiation. At doses exceeding  $175 \text{ mC/cm}^2$ , the Fermi level is moved very deep inside the forbidden band gap and no free carriers can be excited into the conduction and valence bands of the crystal. With further irradiation, the sample remains insulating which supposes that the Fermi level probably stays pinned near mid-gap.

The difference in the observed thermal activation energies in pristine and irradiated samples is apparently related to the Fermi level position. In the pristine sample, it is located between the donor level ( $E_d$ ) and the bottom of conduction band and the Arrhenius plot can be approximated by the so called “half slope” regime<sup>39</sup>  $E_1 \approx E_d/2$ . The sample irradiated at  $160 \text{ mC/cm}^2$  is strongly compensated; the Fermi level is located well below the donor level and the Arrhenius plot is more likely approximated by the “full slope” regime with  $E_2 \approx E_d$ . This situation, which occurs for smaller gap semiconductors, e.g., silicon, at low temperatures, can be realized for large gap semiconductors already at room temperature. As measured in the compensated  $\text{Ga}_2\text{O}_3$  sample, the activation energy  $E_2 = 37 \text{ meV}$  is very close to the value  $36.6 \text{ meV}$  estimated for the shallow-donor ionization energy within the hydrogenic model with  $m_e = 0.28 m_0$  and taking the dielectric constant as  $\varepsilon = 10.2$  (Ref. 40).

The values reported in the literature for the donor activation energies in  $\beta$ -Ga<sub>2</sub>O<sub>3</sub>, obtained from electrical<sup>22,41,42</sup> and EPR measurements<sup>18</sup>, vary over a wide range. Globally, they are found to lie around 20 meV in highly-conducting material and 40 meV in less-conductive samples. Our observations on the same sample where the conductivity is modified by HEE irradiation, suggest to relate this tendency to the degree of donor compensation rather than to conductivity.

In UID samples which have a low initial concentration of conduction electrons, the compensation of donors and the shift of the Fermi level to mid-gap would occur at much lower irradiation doses compared to the highly-doped samples. The changes in the PL spectra of UID samples illustrated in Fig. 13 looks very much like the variation of the free-electron concentration with irradiation (Fig. 4): an almost linear variation at low doses with subsequent saturation above a critical dose. The value of the critical dose, of the order 40 mC/cm<sup>2</sup>, is in fair agreement with the expected downward shift of the Fermi level to mid-gap in such lightly-doped crystals.

The EPR and optical spectra of the UID samples show that the Fermi level downwards shift reveals latent impurity states which were previously screened by the large number of electrons available in the conduction band. It is the case of the EPR lines of TMIs which are very weak in pristine samples but clearly seen in irradiated ones. It is definitely the case of the R-lines in the PL spectrum of irradiated samples. The R-lines luminescence has been reported in numerous publications on chromium doped  $\beta$ -Ga<sub>2</sub>O<sub>3</sub> and attributed to intra-center transitions in Cr<sup>3+</sup> ions<sup>43-47</sup>. This interpretation was definitely established in a recent magneto-optical study where the Zeeman splitting of the R<sub>1</sub>-line under magnetic field was rigorously correlated to the Cr<sup>3+</sup> EPR spectrum<sup>48</sup>. In our

experiments, we observe that the intensity of the  $\text{Cr}^{3+}$  R-lines is very weak in non-irradiated samples and shows a significant growth with increasing irradiation dose (see Figs. 11b and 13). Quite obviously, irradiation does not change the concentration of chromium impurities in the host lattice but it can change the charge state of the impurity ions.  $\text{Cr}^{3+}$  is an isoelectronic impurity replacing a  $\text{Ga}^{3+}$  ion in the host lattice. Apparently, in the presence of a high concentration of free electrons in the conduction band of a *n*-type semiconductor, a  $\text{Cr}^{3+}$  ion can capture an extra electron in its unfilled d-shell. This turns the ion into a state inactive in the PL and EPR spectra of non-irradiated samples. The  $\text{Cr}^{2+}$  (or even  $\text{Cr}^{1+}$ ) ion with a charge less than 3+ would form a negatively charged center in gallium oxide similar to negative -U center in some large band gap semiconductors<sup>49,50</sup>. The energy involved in the charge transfer process can be identified as a donor-like level in the forbidden gap of the semiconductor, besides usual shallow donors related to Sn doping impurities or oxygen vacancies. The formation of negative -U centers on some residual donors in UID  $\text{Ga}_2\text{O}_3$  was identified by quantitative analyses of the temperature variation of EPR-signal intensity<sup>26</sup>.

A possible effect of the variation of the Fermi level on the charge states of impurities was already mentioned based on theoretical considerations<sup>28,51</sup>, its tuning being out of reach; related out-of-equilibrium situations could however be created under optical excitation, leading to experimental data in support of these ideas<sup>52-55</sup>.

The luminescent B-band shows the same behavior as the chromium R-lines, however on a more modest scale. These local centers are already present in the pristine samples and their concentration does not increase very much with irradiation. For the moment we cannot propose a reliable model accounting for the relevant center. We

presume that it also changes its charge state, but the corresponding energy level in the band gap is practically empty in the initial sample so that its population does not change very much with the downward shift of the Fermi level with irradiation.

The introduction of gallium vacancies produces significant changes in the emission spectra but we did not identify any band in the optical spectra which can be directly assigned to these lattice defects. The strong reduction of the total emission intensity with the band-to band excitation in irradiated crystals attests that, with irradiation, we introduce or activate highly-efficient non-radiative recombination centers.

## **IV. CONCLUSIONS**

Irradiation with high-energy electrons induces significant changes in electrical, optical and EPR properties of  $\beta$ -Ga<sub>2</sub>O<sub>3</sub> crystals. All these changes are related to the introduction of gallium vacancies, which act as acceptors thus resulting in a large downwards shift of the Fermi level. In this context HEE irradiation has a potential for converting *n*-type conductivity due to electrons in the conduction band of the initial sample into *p*-type conductivity related to the holes in the valence band. However, up to now we did not yet observe the conductivity type conversion, the sample staying non-conductive up to doses of 250 mC/cm<sup>2</sup>.

The complex problem of the conductivity conversion from *n*- to *p*-type in gallium oxide is largely discussed in the literature<sup>5,56</sup>. Fundamental obstacles for this conversion are: i) very deep level location of all potential acceptors (including V<sub>Ga</sub>), thus preventing the excitation of holes into the valence band at room temperature; ii) self-trapping of holes in crystals with high ionicity: the self-trapped free carriers stay localized and cannot contribute to the electrical conductivity.

## ACKNOWLEDGMENTS

The authors acknowledge the EMIR&A French accelerator network (FR CNRS 3618) for radiation beam time on the SIRIUS platform and support of the Agence de l'Innovation de Défense, Ministère des Armées, under grants 2018 60 0074 00 470 75 01/DIGAO and DIGAO2.

## AUTHOR DECLARATION

The authors have no conflicts to disclose.

## DATA AVAILABILITY

The data that support the findings of this study are available from the corresponding author upon reasonable request.

## REFERENCES

- <sup>1</sup>B. J. Baliga, IEEE Electron Device Lett. **10**, 455 (1989).
- <sup>2</sup>H. W. Xue, Q. M. He, G. Z. Jian, S. B. Long, P. Tao, and M. Liu, Nanoscale Res. Lett. **13**, 290 (2018).
- <sup>3</sup>M. Higashiwaki and S. Fujita, *Gallium Oxide: Materials Properties, Crystal Growth, and Devices* (Springer, Cham, 2020), Vol. 293.
- <sup>4</sup>S. Pearton, F. Ren, and M. Mastro, *Gallium Oxide: Technology, Devices and Applications* (Elsevier, Amsterdam, 2018).
- <sup>5</sup>S. J. Pearton, J. Yang, P. H. Cary, F. Ren, J. Kim, M. J. Tadjer, and M. A. Mastro, Appl. Phys. Rev. **5**, 011301 (2018).
- <sup>6</sup>Z. Galazka, Semicond. Sci. Technol. **33**, 113001 (2018).

- <sup>7</sup>F. Seitz, Discussion Faraday Soc. **5**, 271-282 (1949).
- <sup>8</sup>N. F. Mott, Proc. Roy. Soc. Lond. A **124**, 425 (1929).
- <sup>9</sup>N. F. Mott, Proc. Roy. Soc. Lond. A**135**, 429 (1932).
- <sup>10</sup>K. Cho, M. Konczykowski, S. Teknowijoyo, M. A. Tanatar, and R. Prozorov, Supercond. Sci. Technol. **31**, 064002 (2018).
- <sup>11</sup>A. C. Damask and G. J. Nienes, *Point Defects in Metals* (New York, 1963); Sec. 7, p. 33.
- <sup>12</sup>L. Zhao, M. Konczykowski, H. Deng, I. Korzhovska, M. Begliarbekov, Z. Chen, E. Papalazarou, M. Marsi, L. Perfetti, A. Hruban, and A. Wołoś, Nat. Commun. **7**, 10957 (2016).
- <sup>13</sup>A. Kuramata, K. Koshi, S. Watanabe, Y. Yamaoka, T. Masui, and S. Yamakoshi, Jpn. J. Appl. Phys. **55**, 1202A2 (2016).
- <sup>14</sup><https://portail.polytechnique.edu/lsi/en/facilities/sirius-installation>.
- <sup>15</sup><http://physics.nist.gov/PhysRefData/Star/Text/ESTAR.html>.
- <sup>16</sup>P. Bois, "Etude des défauts ponctuels dans le bismuth," CEA Report No. R-5389 (1987), [https://inis.iaea.org/collection/NCLCollectionStore/\\_Public/18/082/18082185.pdf](https://inis.iaea.org/collection/NCLCollectionStore/_Public/18/082/18082185.pdf).
- <sup>17</sup>O. S. Oen, "Cross sections for atomic displacements in solids by fast electrons," Technical Report, Office of Scientific and Technical Information (OSTI), ID No. 4457758, Report No. ORNL-4897 (1973).
- <sup>18</sup>M. Yamaga, E. G. Viora, K. Shimamura, N. Ichinose, and M. Honda, Phys. Rev. B **68**, 155207 (2003).
- <sup>19</sup>J. B. Varley, J. R. Weber, A. Janotti, and C. G. Van de Walle, Appl. Phys. Lett. **97**, 142106 (2010).
- <sup>20</sup>P. Deak, Q. D. Ho, F. Seemann, B. Aradi, M. Lorke, and T. Frauenheim, Phys. Rev. B. **95**, 075208 (2017).
- <sup>21</sup>Q. D. Ho, T. Frauenheim, and P. Deak, Phys. Rev. B. **97**, 115163 (2018)

- <sup>22</sup>K. Imascher, Z. Galazka, M. Pietsch, R. Uecker, R. Fornari, *J. Appl. Phys.* **110**, 063720 (2011).
- <sup>23</sup>E. Aubay and D. Gourrier, *Phys. Rev. B* **47**, 15023 (1993).
- <sup>24</sup>L. Binet and D. Gourrier, *J. Phys. Chem. Solids*. **59**, 1241 (1998).
- <sup>25</sup>E. G. Vilora, M. Yamaga, T. Inoue, S. Iabasi, Y. Masui, T. Sugawara, and T. Fukuda, *Jpn. J. Appl. Phys.* **41**, L622 (2002).
- <sup>26</sup>N. T. Son, K. Goto, K. Nomura, Q. T. Thieu, R. Togashi, H. Murakami, Y. Kumagai, A. Kuramata, M. Higashiwaki, A. Koukitu, S. Yamakoshi, B. Monemar, and E. Janzén, *J. Appl. Phys.* **120**, 235703 (2016).
- <sup>27</sup>B. E. Kananen, L. E. Halliburton, K. T. Stevens, G. K. Foundos, and N. C. Gilles, *Appl. Phys. Lett.* **110**, 202104 (2017).
- <sup>28</sup>H. J. von Bardeleben, S. Zhou, U. Gerstmann, D. Skachkov, W. R. L. Lambrecht, Q. D. Ho, and P. Deák, *Appl. Phys. Lett. Mater.* **7**, 022521 (2019).
- <sup>29</sup>N. T. Son, Q. D. Ho, K. Goto, H. Abe, T. Ohshima, B. Monemar, Y. Kumagai, T. Frauenheim, and P. Deak, *Appl. Phys. Lett.* **117**, 032101 (2020).
- <sup>30</sup>G. Blasse and A. Brill, *J. Phys. Chem. Solids*. **31**, 707 (1970).
- <sup>31</sup>T. Harwig, F. Kellendonk, and S. Slappendel, *J. Phys. Chem. Solids* **39**, 675 (1978).
- <sup>32</sup>T. Harwig and F. Kellendonk, *J. Solid State. Chem.* **24**, 255 (1978).
- <sup>33</sup>T. Onuma, Y. Nakata, K. Sasaki, T. Masui, Y. Yamaguchi, T. Honda, A. Kuramata, S. Yamakoshi, and M. Hishasiwaki, *J. Appl. Phys.* **124**, 075103 (2018).
- <sup>34</sup>Q. D. Ho, T. Frauenheim, and P. Deak, *Phys. Rev. B* **97**, 115163 (2018).
- <sup>35</sup>Y. K. Frodason, K. M. Johansen, L. Vines, and J. B. Varley, *J. Appl. Phys.* **127**, 075701 (2020).

- <sup>36</sup>T. Onuma, S. Fujioka, T. Yamaguchi, M. Higashiwaki, K. Sasaki, T. Masui and T. Honda, Appl. Phys. Lett. **103**, 041910 (2013).
- <sup>37</sup> Y. Wang, P. T. Dickens, J. B. Varley, X. Ni, E. Lotubai, S. Sprawls, F. Liu, V. Lordi, S. Krishnamoorthy, S. Blair, K. G. Lynn, M. Scarpulla, and Sensale-Rodriguez, Sci. Rep. **8**, 18075 (2018).
- <sup>38</sup>T. Onuma, S. Saito, K. Sasaki, T. Masui, T. Yamaguchi, T. Honda, and M. Higashiwaki, Jpn. J. Appl. Phys. **54**, 112601 (2015).
- <sup>39</sup>M. D. McCluskey and E. E. Haller “*Dopants and defects in semiconductors*,” CRC press, (2018).
- <sup>40</sup>B. Hoeneisen, C. A. Mead, and M.-A. Nicolet, Solid-State Electron. **14**, 1057 (1971).
- <sup>41</sup>M. R. Lorenz, J. F. Woods, and R. J. Cambino, J. Phys. Chem. Solids **28**, 403 (1967).
- <sup>42</sup>Z. Galazka, R. Uecker, K. Irmischer, M. Albrecht, D. Klimm, M. Pietsch, M. Brutzam, R. Bertram, S. Ganschow, and R. Fornari, Cryst. Res. Technol. **45**, 1229 (2010).
- <sup>43</sup>H. H. Tippins, Phys. Rev. **137**, A865 (1965).
- <sup>44</sup>G. P. Morgan, T. J. Glynn, G. F. Imbusch, and J. P. Remeika, J. Chem. Phys. **69**, 4859 (1978).
- <sup>45</sup>Y. Tokida and S. Adachi, J. Appl. Phys. **112**, 063522 (2012).
- <sup>46</sup>A. Luचेchko, V. Vasylytsiv, Y. Zhydashkevskyy, M. Kushlyk, S. Ubizskii, and A. Suchocki, J. Phys. D: Appl. Phys. **53**, 354001 (2020).
- <sup>47</sup> G. Naresh-Kumar, H. MacIntyre, S. Subashchandran, P. R. Edwards, R. W. Martin, K. Daivasigamani, K. Sasaki, and A. Kuramata, Phys. Stat. Sol. (b), **258**, 2000465 (2021).
- <sup>48</sup>I. E. Stehr, M. Jansson, D. M. Hofmann, J. Kim, S. J. Pearton, W. M. Chen, and I. A. Buyanova, Appl. Phys. Lett. **119**, 052101 (2021).
- <sup>49</sup>D. J. Chadi and K. J. Chang, Phys. Rev. Lett. **61**, 873 (1988).

- <sup>50</sup>X. T. Trinh, D. Nilsson, I. G. Ivanov, E. Janzen, A. Kakanakova-Georgieva, and N. T. Son, Appl. Phys. Lett. **108**, 162106 (2014).
- <sup>51</sup>D. Skachkov, W. R. L. Lambrecht, H. J. von Berdeleben, U. Gerstmann, Q. D. Ho, and P. Deák, J. Appl. Phys. **125**, 185701 (2019).
- <sup>52</sup>C. A. Lenyk, T. D. Gustafson, L. E. Halliburton, and N. C. Giles, J. Appl. Phys. **126**, 245701 (2019).
- <sup>53</sup>C. A. Lenyk, N. C. Giles, E. M. Scherrer, B. E. Kananen, L. E. Halliburton, K. T. Stevens, G. K. Foundos, J. D. Blevins, D. L. Dorsey, and S. Mou, J. Appl. Phys. **125**, 045703 (2019).
- <sup>54</sup>T. D. Gustafson, C. A. Lenyk, L. E. Halliburton, and N. C. Giles, J. Appl. Phys. **128**, 145704 (2020).
- <sup>55</sup>T. D. Gustafson, N. C. Giles, B. C. Holloway, C. A. Lenyk, J. Jesenovec, J. S. McCloy, M. D. McCluskey, and L. E. Halliburton, J. Appl. Phys. **131**, 065702 (2022).
- <sup>56</sup>A. Kyrtos, M. Matsubara, and E. Bellotti, Appl. Phys. Lett, **112**, 032108 (2018).